

Systematic deviations from Gaussianity in models of quasigeostrophic turbulence

I. Timofeyev^{a)}

Department of Mathematics, University of Houston, Houston, Texas 77204, USA

(Received 7 June 2007; accepted 16 October 2007; published online 29 November 2007)

Microcanonical simulations of spectral truncations of the barotropic quasigeostrophic model are utilized to demonstrate systematic departures from Gaussianity in these models. Truncated equations conserve both the energy and the enstrophy, and predictions of the equilibrium statistical theory are Gaussian for all values of geophysical parameters. Nevertheless, nonzero topographic modes induce significant departures from Gaussianity in corresponding Fourier wavenumbers of the stream function. In particular, the distribution becomes asymmetric, resulting in a significant increase of the third moment. This behavior is most noticeable for large-scale topographic components (with small wavenumbers) and intermediate truncation sizes. © 2007 American Institute of Physics.

[DOI: 10.1063/1.2815728]

I. INTRODUCTION

Equilibrium statistical theories have been successfully utilized in many areas of physics and mathematics, and, in particular, in fluid dynamics. This approach predicts the equilibrium statistical state of the fluid given the values of several essential constraints of the flow. In particular, equilibrium statistical theory has been utilized in the context of the atmosphere and ocean dynamics¹⁻⁶ and to explain the statistical behavior of Jupiter's red spot.^{7,8} Various promising statistical strategies were also developed to model small-scale processes.^{9-13,5} These statistical theories are typically utilized in various subgrid-scale parametrizations and to explain the statistical behavior of large scales.

Gaussianity is one of the most common and natural assumptions in statistical physics and fluid dynamics. A vast literature exists supporting this assumption, which has been successfully utilized in many cases. On the other hand, it also has been recognized that non-Gaussianity can appear naturally in numerical and observational data. It was demonstrated that additional conserved quantities in specially designed low-dimensional truncations of the two-dimensional vorticity equation can lead to non-Gaussian statistical behavior.^{14,15} Also, truncations with higher-order Casimir invariants were examined in Refs. 16 and 17. It was demonstrated that higher-order invariants are relevant for small to intermediate truncation sizes and can result in non-Gaussian behavior of the large scales.

It also has been recognized that the underlying bottom topography can have a profound affect on large scales.^{2,18,5} Here we examine the role of the underlying bottom topography in statistical predictions for quasigeostrophic flows. In particular, we demonstrate that statistical properties of the large scales can deviate from Gaussian predictions of the equilibrium statistical theory with two conserved quantities, namely the energy and the enstrophy. Microcanonical simu-

lations of the truncated barotropic quasigeostrophic model with small to intermediate truncation sizes demonstrate that nonzero topographic Fourier wavenumbers can cause significant skewness in the corresponding modes of the stream function.

The rest of the paper is organized as follows. In Sec. II, we introduce the model, briefly discuss its analytical properties, and outline the application of the equilibrium statistical mechanics. Then, in Secs. III and IV we analyze the model numerically with several choices of the bottom topography and with and without other geophysical effects, such as the mean flow and the Coriolis parameter.

II. THE MODEL

The nondimensional form of the barotropic quasigeostrophic model can be written through the small-scale stream functions $\psi(x, t)$ and the zonal mean flow $U(t)$,

$$\partial_t q + \nabla^\perp \psi \cdot \nabla q + U(t) \partial_x q + \beta \partial_x \psi = 0,$$

$$q = \Delta \psi + h = \omega + h, \quad (1)$$

$$\dot{U} = \frac{1}{4\pi^2} \int h \partial_x \psi dx dy,$$

where the zonal mean flow, $U(t)$, interacts with small-scale eddies via the topographic stress, β approximates variation of the Coriolis parameter, $h = h(x, y)$ represents the underlying bottom topography, and $\nabla^\perp \psi = (-\partial_y \psi, \partial_x \psi)$ is the small-scale velocity field. We consider the equations in (1) in the $2\pi \times 2\pi$ doubly periodic domain, thus the topography is also chosen to be periodic with mean zero. The equations in (1) conserve two quadratic invariants, namely the energy and the enstrophy,

$$E = \frac{1}{2} U^2 + \frac{1}{2} \int |\nabla \psi|^2 dx,$$

^{a)}Electronic mail: ilya@math.uh.edu. Telephone: 713-743-3483. Fax: 713-743-3505.

TABLE I. Number of real degrees of freedom in the spectral truncation of the stream function, ψ_Λ , with the spectral projection in Eq. (4).

Truncation size, Λ	4	6	8	10	15	20
Real degrees of freedom in ψ_Λ	40	84	144	220	480	840

$$\mathcal{E} = \beta U + \frac{1}{2} \int |q|^2 dx,$$

respectively. Details of the derivation are provided, for example, in Ref. 5.

It is natural to consider the spectral representation of the equations in (1). With the expansion

$$\psi(x, t) = \sum_{\mathbf{k}} \psi_{\mathbf{k}}(t) e^{i\mathbf{k}\cdot\mathbf{x}},$$

the equations in (1) can be rewritten as an infinite system of ordinary differential equations for the Fourier coefficients of the stream function, $\psi_{\mathbf{k}}$, and the mean flow, $U(t)$,

$$\begin{aligned} \dot{\psi}_{\mathbf{k}} = & \frac{1}{2} \sum_{\mathbf{k}+\mathbf{l}+\mathbf{m}=0} B_{\mathbf{k}\mathbf{l}\mathbf{m}} \psi_{\mathbf{l}}^* \psi_{\mathbf{m}}^* + \sum L_{\mathbf{k}\mathbf{l}} \psi_{\mathbf{l}} + i(\Omega_{\mathbf{k}} - k_x U) \psi_{\mathbf{k}} \\ & + iH_{\mathbf{k}} U, \end{aligned} \quad (2)$$

$$\dot{U} = \text{Im} \sum k_x h_{\mathbf{k}} \psi_{\mathbf{k}}^*,$$

where

$$B_{\mathbf{k}\mathbf{l}\mathbf{m}} = (l_y m_x - l_x m_y) \frac{|\mathbf{l}|^2 - |\mathbf{m}|^2}{|\mathbf{k}|^2}, \quad L_{\mathbf{k}\mathbf{l}} = (l_y k_x - l_x k_y) \frac{h_{\mathbf{k}-\mathbf{l}}}{|\mathbf{l}|^2},$$

$$\Omega_{\mathbf{k}} = \frac{k_x \beta}{|\mathbf{k}|^2}, \quad H_{\mathbf{k}} = \frac{k_x h_{\mathbf{k}}}{|\mathbf{k}|^2},$$

\mathbf{k} , \mathbf{l} , and \mathbf{m} are two-dimensional wavenumbers, i.e., $\mathbf{k} = (k_x, k_y)$, etc., and $h_{\mathbf{k}}$ are the Fourier coefficients of the topography. In addition, all Fourier coefficients obey the reality condition

$$\psi_{\mathbf{k}}^* = \psi_{-\mathbf{k}}. \quad (3)$$

Here we consider the spectral projection of the equations in (2) on the ‘‘triangular’’ Fourier domain

$$T_\Lambda = \{\mathbf{k} = (k_x, k_y) : |k_x| + |k_y| \leq \Lambda\}, \quad (4)$$

i.e., we consider the system in Eq. (2) with all wavenumbers restricted to the set T_Λ ,

$$\mathbf{k}, \mathbf{l}, \mathbf{m} \in T_\Lambda. \quad (5)$$

Truncated equations (2) and (5) satisfy the Liouville (volume-preserving) property. In addition, the system in Eqs. (2) and (5) conserves discrete analogs of energy and enstrophy (see Ref. 5),

$$E_\Lambda = \frac{1}{2} U^2 + \frac{1}{2} \sum_{\mathbf{k} \in T_\Lambda} |\mathbf{k}|^2 |\psi_{\mathbf{k}}|^2, \quad (6)$$

$$\mathcal{E}_\Lambda = \beta U + \frac{1}{2} \sum_{\mathbf{k} \in T_\Lambda} (|\mathbf{k}|^2 \psi_{\mathbf{k}} - h_{\mathbf{k}})^2, \quad (7)$$

for any symmetric truncation. Therefore, it has been recognized that the equilibrium statistical mechanics formalism is applicable to various spectral truncations of the system in Eq. (1) and its analogs in spherical geometry.^{3,4} The prediction of the equilibrium statistical mechanics is the probability measure, which maximizes the Shannon entropy,

$$S(p) = \int_{R^N} p(\mathbf{Z}) \ln p(\mathbf{Z}) d\mathbf{Z},$$

given the constraints for the invariants of the flow

$$\langle E_\Lambda \rangle = \overline{E_\Lambda}, \quad \langle \mathcal{E}_\Lambda \rangle = \overline{\mathcal{E}_\Lambda}, \quad (8)$$

where \mathbf{Z} is the vector of dependent variables in the truncation, and averages are taken with respect to the probability distribution $p(\mathbf{Z})$. Due to the reality condition (3), not all the wavenumbers in the truncation are independent. Therefore, the vector of the dependent variables can be described as $\mathbf{Z} = (U, \text{Re} \psi_{\mathbf{k}}, \text{Im} \psi_{\mathbf{k}})$ with $\mathbf{k} \in T_\Lambda$ and satisfying $\{\mathbf{k} \in \mathbf{Z} \Rightarrow -\mathbf{k} \notin \mathbf{Z}\}$. For example, the following choice describes all independent degrees of freedom in the truncation $\mathbf{Z} = (U, \text{Re} \psi_{\mathbf{k}}, \text{Im} \psi_{\mathbf{k}})$ with $\{\mathbf{k} \in T_\Lambda, k_x > 0\} \cup \{(0, \mathbf{k}_y), 0 < k_y \leq \Lambda\}$. Number of independent degrees of freedom in ψ_Λ for truncation sizes considered in this paper is presented in Table I.

Utilizing the Lagrange multiplier method, the prediction for the distribution of \mathbf{Z} can be computed explicitly as

$$p(\mathbf{Z}) = C \exp(-\theta_1 E_\Lambda - \theta_2 \mathcal{E}_\Lambda),$$

where C is the normalization constant, and $\theta_{1,2}$ are the Lagrange multipliers to satisfy the constraints in Eq. (8). Since the invariants in Eqs. (6) and (7) are quadratic, this yields a two-parameter family of multivariate Gaussians for the distribution of $\psi_{\mathbf{k}}$ and U . Therefore, the statistical behavior of the dependent variables is completely determined by their means and variances,

$$\text{mean } U = -\frac{\beta}{\mu}, \quad \text{var } U = \frac{1}{\alpha\mu}, \quad (9)$$

$$\text{mean } \psi_{\mathbf{k}} = \frac{h_{\mathbf{k}}}{\mu + |\mathbf{k}|^2}, \quad \text{var } \psi_{\mathbf{k}} = \frac{1}{\alpha|\mathbf{k}|^2(\mu + |\mathbf{k}|^2)}, \quad (10)$$

where $\alpha, \mu > 0$ are two parameters related to the energy-enstrophy level (same as to the Lagrange multipliers $\theta_{1,2}$) in the system. Details of this derivation are presented in Ref. 5. We would like to point out that according to the equilibrium distribution, the magnitude of the topography affects only the mean of the corresponding Fourier mode of the stream func-

tion. The equilibrium prediction for the third moment is zero for all variables, i.e., if we define the skewness

$$\text{skew}f = \frac{\langle (f - \bar{f})^3 \rangle}{\langle (f - \bar{f})^2 \rangle^{3/2}}$$

as the measure of the asymmetry of the distribution, then the equilibrium prediction is

$$\text{skew}U = \text{skew}\psi_{\mathbf{k}} = 0. \quad (11)$$

The total energy and the total enstrophy of the system can be decomposed into the mean part and the fluctuating part, and the energy–enstrophy constraints can be expressed through parameters α and μ as follows:

$$\langle E_{\Lambda} \rangle = E_{\Lambda}^{\text{mean}} + E_{\Lambda}^{\text{fluc}}, \quad \langle \mathcal{E}_{\Lambda} \rangle = \mathcal{E}_{\Lambda}^{\text{mean}} + \mathcal{E}_{\Lambda}^{\text{fluc}},$$

with

$$E_{\Lambda}^{\text{mean}} = \frac{\beta^2}{2\mu^2} + \frac{1}{2} \sum_{\mathbf{k} \in T_{\Lambda}} \frac{|\mathbf{k}|^2 |h_{\mathbf{k}}|^2}{(\mu + |\mathbf{k}|^2)^2}, \quad (12)$$

$$E_{\Lambda}^{\text{fluc}} = \frac{1}{2\alpha\mu} + \frac{1}{2\alpha} \sum_{\mathbf{k} \in T_{\Lambda}} \frac{1}{\mu + |\mathbf{k}|^2},$$

$$\mathcal{E}_{\Lambda}^{\text{mean}} = -\frac{\beta^2}{\mu} + \frac{1}{2} \sum_{\mathbf{k} \in T_{\Lambda}} \frac{\mu^2 |h_{\mathbf{k}}|^2}{(\mu + |\mathbf{k}|^2)^2}, \quad (13)$$

$$\mathcal{E}_{\Lambda}^{\text{fluc}} = \frac{1}{2\alpha} \sum_{\mathbf{k} \in T_{\Lambda}} \frac{|\mathbf{k}|^2}{\mu + |\mathbf{k}|^2}.$$

In Eqs. (12) and (13), terms outside of the summations [i.e., $\beta^2/(2\mu^2)$, $1/(2\alpha\mu)$, and $-\beta^2/\mu$] correspond to the contribution of the mean flow, U . These terms should be omitted when the mean flow is not present in the model (i.e., $\beta=U=0$).

The above formalism was developed for the ensemble predictions of the system. However, the key question is the applicability of this approach to the microcanonical simulations on a constant energy–enstrophy level consistent with the constraint in (8). Some numerical evidence suggests that the ergodicity assumption holds for the truncated system in (2) with (4) and time averages in microcanonical simulations converge to the predictions of the equilibrium statistical theory in (9) and (10). Nevertheless, the majority of the literature concentrates on the statistical predictions for means and variances of the dependent variables. Here we demonstrate that, indeed, the first two moments are in good agreement with the statistical predictions in (9) and (10), but the skewness of the distribution is strongly affected by the presence of the underlying bottom topography.

III. STATISTICAL BEHAVIOR FOR $\beta=U=0$

For the barotropic model, the zonal mean flow is, typically, induced by various geophysical effect, such as the Earth's rotation. Therefore, we first consider a simplified system with $\beta=U=0$ in Eqs. (1) and (2) for all times. The motivation here is to demonstrate that the deviations from Gaussianity are not related to the variations of the Coriolis

parameter and/or interactions between the mean flow and small-scale eddies. In addition, results reported here indicate that energy and enstrophy are two main conserved quantities determining the statistical properties of the stream function. Even if other conserved quantities exist in the truncated model, they do not seem to have a strong influence on the overall trend in the statistical behavior of the stream function.

With the simplification $\beta=U=0$, the equations in (2) and (5) reduce to

$$\dot{\psi}_{\mathbf{k}} = \frac{1}{2} \sum_{\mathbf{k}+\mathbf{l}+\mathbf{m}=0} B_{\mathbf{k}\mathbf{l}\mathbf{m}} \psi_{\mathbf{l}}^* \psi_{\mathbf{m}}^* + \sum L_{\mathbf{k}\mathbf{l}} \psi_{\mathbf{l}}, \quad \mathbf{k}, \mathbf{l}, \mathbf{m} \in T_{\Lambda} \quad (14)$$

with truncated analogs of energy and enstrophy

$$E_{\Lambda} = \frac{1}{2} \sum_{\mathbf{k} \in T_{\Lambda}} |\mathbf{k}|^2 |\psi_{\mathbf{k}}|^2, \quad (15)$$

$$\mathcal{E}_{\Lambda} = \frac{1}{2} \sum_{\mathbf{k} \in T_{\Lambda}} \|\mathbf{k}\|^2 |\psi_{\mathbf{k}} - h_{\mathbf{k}}|^2, \quad (16)$$

and the equilibrium statistical prediction is still a family of Gaussians with means and variances in Eqs. (10), and the skewness being zero.

We verify the equilibrium predictions for the Fourier coefficients of the stream function by integrating equations in Eq. (14) numerically. Parameters α and μ in Eqs. (10) are chosen to be

$$\alpha = 1, \quad \mu = 2. \quad (17)$$

The stream function is initialized at random on a fixed energy–enstrophy level consistent with the constraints in Eqs. (12) and (13) for the above choice of parameters α and μ and all statistics are computed as time averages from a single microcanonical realization. The equations in (14) were integrated utilizing the pseudospectral method in space and fourth-order Runge–Kutta time-stepping in time for the total time $T=365,000$, skipping $t_0=5,000$ in statistical calculations to ensure statistical equilibration. In addition, we also selectively (for some truncation sizes and topographic magnitudes) verified that different initial data with identical energy–enstrophy constraints lead to the same statistical behavior.

A. Single-mode topography

First, we investigate the equations in (14) with a single-mode topography

$$h(x, y) = H_0 [\cos(x + 2.31) + \sin(x + 0.11)], \quad (18)$$

with several values of H_0 , such that

$$\max|h| = 0, 0.42, 0.5, 1, 1.5, 2.$$

In addition, four truncation sizes,

$$T_{\Lambda}, \quad \Lambda = 4, 6, 8, 10, \quad (19)$$

are considered. The only nonzero coefficients of the topography (18) are

TABLE II. DNS: Numerical and analytical prediction for the low-order moments of ψ_k in simulations of the equation in (14) with topography (18), $\max|h|=1$ and $\Lambda=6$.

	Num Mean	StatMech Mean	Num Var	StatMech Var	Num Skewness	Num Flatness
Re $\psi_{1,0}$	-0.137631	-0.152259	0.176	0.1666	0.24184	2.58
Re $\psi_{0,1}$	-0.001702	0	0.1774	0.1666	-0.0017	2.5
Re $\psi_{1,1}$	0.000917	0	0.0679	0.0625	0.00092	2.66
Re $\psi_{1,-1}$	0.001288	0	0.0681	0.0625	0.053	2.72
Re $\psi_{2,0}$	0.000438	0	0.0221	0.0208	-0.0334	2.88
Re $\psi_{0,2}$	-0.000036	0	0.0222	0.0208	-0.0746	2.86

$$h_{\pm 1,0} = (-0.457 \mp 0.21i)H_0, \quad (20)$$

consistent with the reality condition (3).

Overall, predictions of the statistical mechanics in Eqs. (10) for the system in Eq. (14) are confirmed with high accuracy for all modes ψ_k in the absence of the topographic mode $h_{1,0}$. Moreover, the first two moments exhibit a good agreement with analytical predictions of the equilibrium statistical mechanics in Eqs. (10) even when the topography is present. These results are consistent with findings reported in Refs. 1, 2, and 5. As an example, a comparison of numerical and analytical predictions for $\Lambda=6$ and $\max|h|=1$ is presented in Table II. On the other hand, when a particular topographic mode is nonzero ($h_{1,0}$ in the present case), the skewness of the corresponding stream function's Fourier mode deviates significantly from Gaussianity (i.e., zero). This is illustrated in Fig. 1, where the distribution of Re $\psi_{1,0}$ is depicted for $\Lambda=6$ and $\max|h|=1.5$. The distribution of Re $\psi_{1,0}$ is tilted to the left, which corresponds to the positive skewness of the distribution. Moreover, the magnitude of the third moment is proportional to the height of the topography. The linear relationship between the magnitude of the topographic wavenumber $h_{1,0}$ and the skewness of Re $\psi_{1,0}$ holds for topographies of small to intermediate magnitudes. This behavior is illustrated in Fig. 2.

graphic wavenumber $h_{1,0}$ and the skewness of Re $\psi_{1,0}$ holds for topographies of small to intermediate magnitudes. This behavior is illustrated in Fig. 2.

We also investigated the dependence of the third moment on the size of the truncation. In this series of simulations, four truncation sizes in Eq. (19) were considered, while the magnitude of the topography (18) was kept constant with $\max|h|=1$. These results are depicted in Fig. 3. The skewness of the distribution of $\psi_{1,0}$ decreases with Λ and roughly follows the $-1/2$ power law. Therefore, we expect that for higher resolutions, the distribution of $\psi_{1,0}$ approaches the Gaussian prediction in Eqs. (10) and (11). Nevertheless, this approach is slow and non-Gaussian features are noticeable for all intermediate size truncations.

B. Higher-frequency single-mode topographies

Next, we investigate the behavior of the system in Eq. (14) for single-mode topographies with a higher topographic mode. In particular, the following topographies are considered:

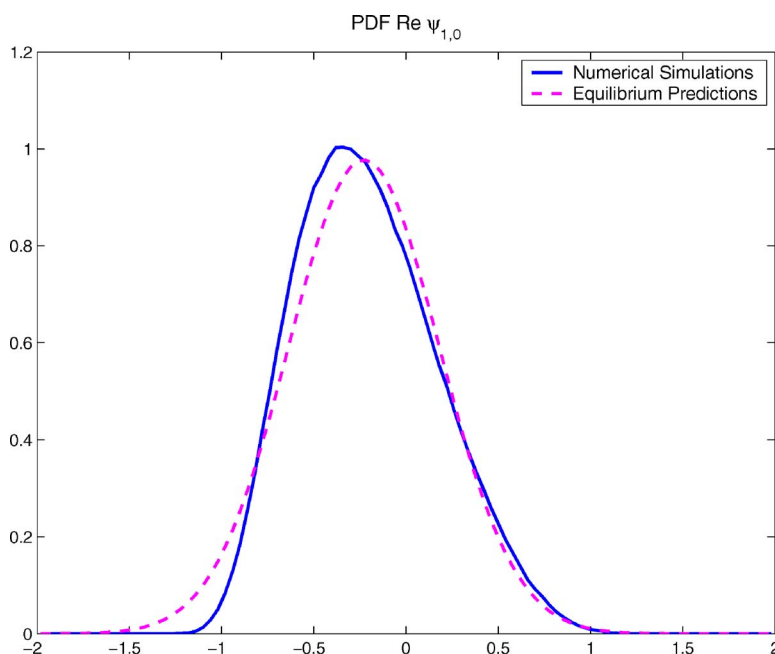


FIG. 1. (Color online) Distribution of the Fourier component Re $\psi_{1,0}$ in the simulations of the truncated system (14) with $\Lambda=6$ and topography (18) with $\max|h|=1.5$.

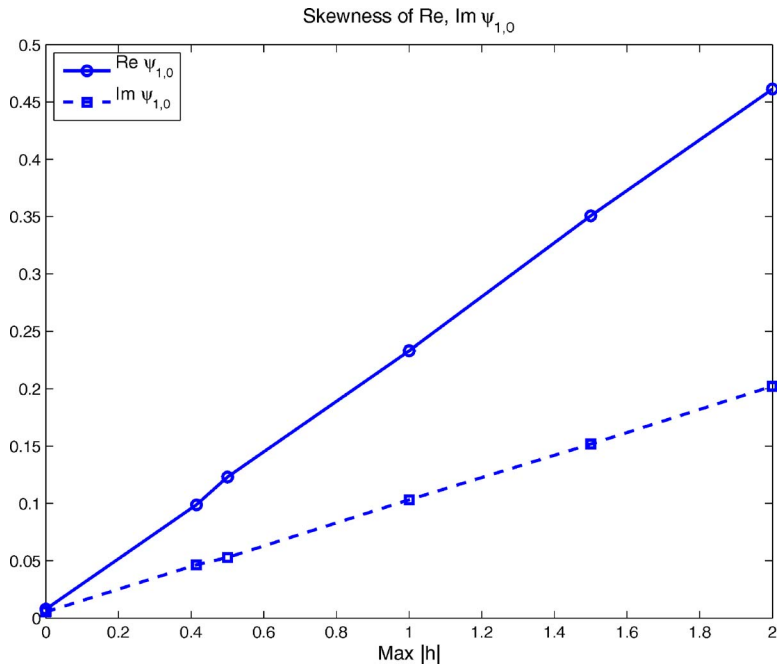


FIG. 2. (Color online) Skewness of the Fourier component $\psi_{1,0}$ in the simulations of the truncated system (14) with $\Lambda=6$ and topography (18) vs the magnitude of the topography.

$$h_{\mathbf{k}}(x,y) = H_0\{\cos[\mathbf{k} \cdot (x,y) + 0.4] + \sin[\mathbf{k} \cdot (x,y) + 1.28]\} \quad (21)$$

with $\mathbf{k}=(1,0), (1,1), (2,0), (2,1)$, and several values of H_0 , so that

$$\max|h| = 0.63, 1.26, 1.89, 2.52, 3.78, 5.04, 6.3.$$

We would like to emphasize that in each simulation, only one topographic mode \mathbf{k} is present with the corresponding nonzero Fourier coefficients $h_{\pm\mathbf{k}}=H_0(0.63\pm 0.034i)$, and the magnitude of topographies (21) depends only on the particular value of H_0 , and is independent of the wavenumber, \mathbf{k} . Due to the significant difference in the magnitude of the real and imaginary parts of the topographic mode, $h_{\mathbf{k}}$, deviations from Gaussianity are manifested more strongly for the real part of the corresponding Fourier coefficient of the stream

function. We also would like to emphasize that the maximum magnitude of the topography is much larger than in simulations in the preceding section (depicted in Fig. 2).

The skewness of the corresponding Fourier coefficient of the stream function, $\text{Re } \psi_{\mathbf{k}}$, is plotted against the magnitude of the topography in Fig. 4. The topographic mode induces significant deviation from the Gaussian predictions for all wavenumbers considered in this section. On the other hand, the non-Gaussian effect of the topography weakens for higher topographic modes. In particular, for higher topographic wavenumbers, the skewness of the corresponding Fourier coefficients of the stream function is smaller than for the topography of the same magnitude with a lower frequency. In addition, the third moment grows slower for

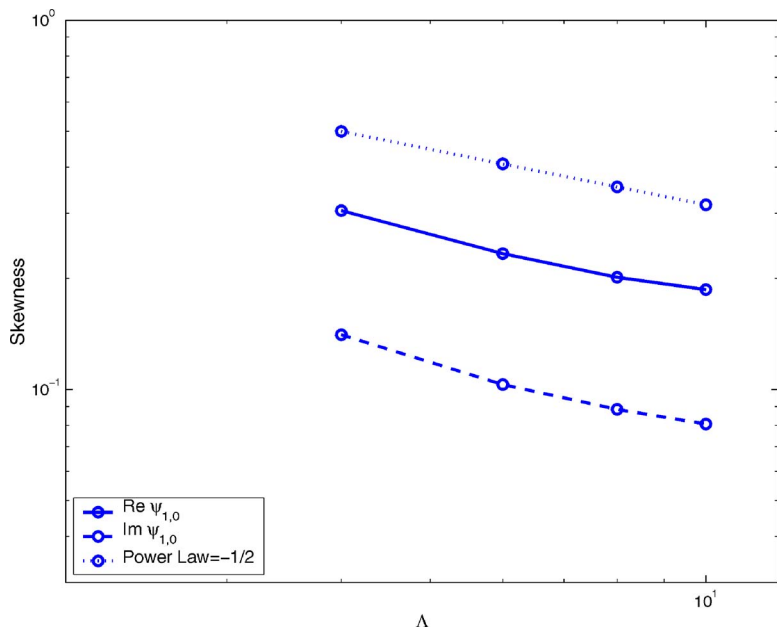


FIG. 3. (Color online) Log-log plot of the skewness of the Fourier component $\psi_{1,0}$ in the simulations of the truncated system (14) with topography (18) and different truncation sizes T_{Λ} , with $\Lambda=4,6,8,10$.

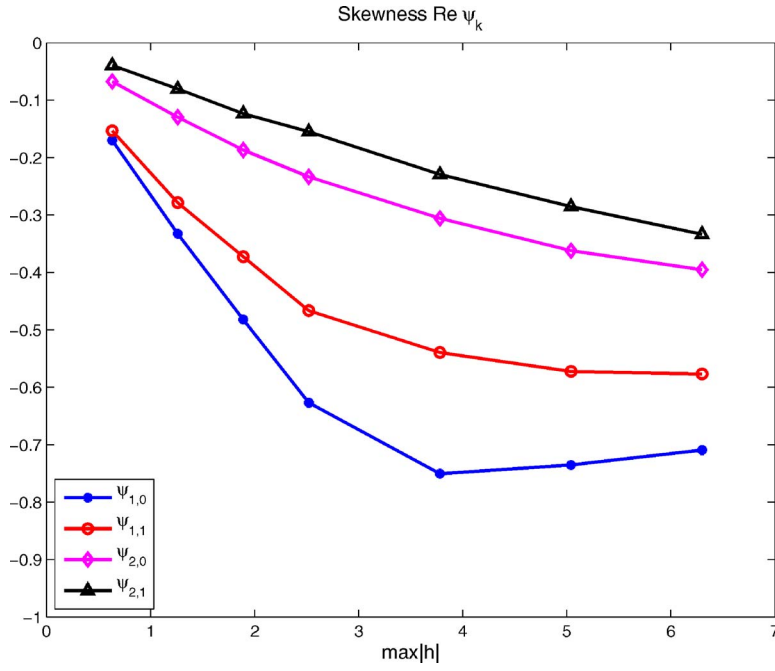


FIG. 4. (Color online) Skewness of the Fourier component ψ_k in the simulations of the truncated system (14) with topography (21) and different magnitudes H_0 .

higher topographic spectral components. Finally, we also observe the saturation of the skewness when the topography becomes too large.

Overall, simulations with single-mode topographies (21) can be summarized as follows: (i) Means and variances of the Fourier coefficients ψ_k are in good agreement with the predictions of the equilibrium statistical mechanics, and (ii) nonzero topographic modes induce significant departures from Gaussianity for the third moment in low-dimensional truncations of the barotropic quasigeostrophic model. In addition, these simulations also demonstrate that (iii) the signature of the non-Gaussian behavior weakens as the topographic Fourier frequency or the size of the truncation are increased and (iv) the third moment is linearly proportional to the magnitude of h for small h , but skewness growth saturates for larger magnitudes.

C. Multimode topographies

To investigate the interaction of topographic modes, we consider the statistical behavior of the truncated system in (14) with multimode topographies,

$$h(x, y) = H_0 \{ \cos(x + 2.31) + \sin(x + 0.11) - \cos(2x - 1.7) + \sin(2x + 0.3) + M_0 [\cos(x + y + 2.8) - \sin(x + y + 1.55)] \} \quad (22)$$

with

$$H_0 = 0.67, \quad M_0 = 0, 1, 2, 3.$$

The phase of the Fourier coefficient $h_{1,0}$ coincides with the single-mode topography considered in (18). In addition, two more frequencies, (1,1) and (2,0), are introduced. The magnitude of the single-mode topography in (18) with $H_0=0.67$ is approximately 0.42. Therefore, we can compare the behavior of the mode $\psi_{1,0}$ with simulations in the preceding section. The magnitude of the topographic mode (1,1) is varied

to demonstrate interactions between various topographic frequencies. The statistical behavior of $\psi_{1,0}$ and $\psi_{1,1}$ versus M_0 is presented in the top part of Table III and also in Fig. 5. We would like to emphasize that the maximum magnitude of the topography (22) varies from $\max|h_{M_0=0}|=0.68$ to $\max|h_{M_0=3}|=4.65$. Simulations with multimode topographies (22) demonstrate that the statistical behavior of the Fourier mode $\psi_{1,0}$ is affected by the magnitude of the topographic mode $h_{1,1}$. The mean and the skewness of the mode $\psi_{1,0}$ are affected especially strongly by the growth of the topographic mode $h_{1,1}$. The total changes in the mean and the skewness of $\text{Re } \psi_{1,0}$ are approximately 15% and 25%, respectively.

TABLE III. Statistics of the Fourier components $\psi_{1,0}$, $\psi_{1,1}$, and the mean flow U in simulations with topography (22) with and without U and β .

	$M_0=0$	$M_0=1$	$M_0=2$	$M_0=3$
$U, \beta=0$				
Mean Re $\psi_{1,0}$	-0.05462	-0.05741	-0.06038	-0.06126
Var Re $\psi_{1,0}$	0.15528	0.15626	0.16152	0.16467
Skew Re $\psi_{1,0}$	0.10291	0.09357	0.08309	0.06283
Mean Re $\psi_{1,1}$	0.00014	-0.16147	-0.32829	-0.4970
Var Re $\psi_{1,1}$	0.06296	0.05742	0.04455	0.03193
Skew Re $\psi_{1,1}$	-0.00291	0.28019	0.45894	0.53036
$U, \beta \neq 0$				
Mean Re $\psi_{1,0}$	-0.053873	-0.05413	-0.05677	-0.05904
Var Re $\psi_{1,0}$	0.151778	0.15325	0.15701	0.161
Skew Re $\psi_{1,0}$	0.08291	0.08074	0.06686	0.05299
Mean Re $\psi_{1,1}$	0.000093	-0.15428	-0.31496	-0.48003
Var Re $\psi_{1,1}$	0.061	0.05661	0.04658	0.03569
Skew Re $\psi_{1,1}$	-0.002985	0.22866	0.38482	0.48092
Mean U	-0.1753	-0.186186	-0.191914	-0.204916
Var U	0.374507	0.381094	0.401869	0.420441
Skew U	0.24062	0.241252	0.223465	0.197856

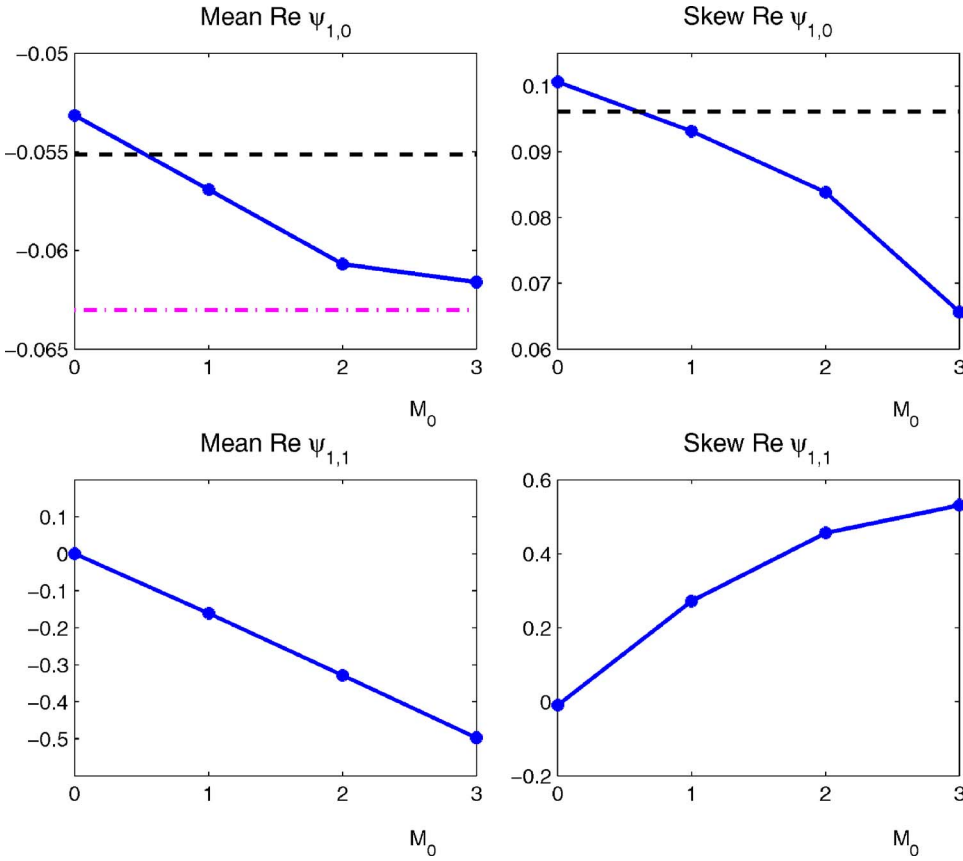


FIG. 5. (Color online) Simulations with the multimode topography in (22) with $U=\beta=0$. Top left: Solid line, mean of $\text{Re } \psi_{1,0}$; dashed and dashed-dotted lines, comparison with simulations with the single-mode topography in (18) with $H_0=0.67$ and predictions of the equilibrium statistical mechanics, respectively. Top right: Solid line, skewness of $\text{Re } \psi_{1,0}$; dashed line, comparison with simulations with the single-mode topography in (18) with $H_0=0.67$. Bottom left and right: Mean and skewness of $\text{Re } \psi_{1,1}$, respectively.

The statistics of the mode $\psi_{2,0}$ exhibit a similar (but less pronounced) trend, and are not presented here for brevity of presentation. The mean of $\psi_{1,1}$ grows linearly with M_0 , as expected, but the skewness exhibits a sublinear growth, similar to the simulations in Sec. III B with large single-mode topographies. In addition to significant deviations from Gaussianity in modes where the topography is nonzero, simulations in this section also demonstrate a strong influence of the topographic mode $h_{1,1}$ on the mean and the skewness of $\psi_{1,0}$, which are only significant when the topographic mode $h_{1,0}$ is present. Therefore, topographic frequencies interact in a nontrivial manner and can have a strong affect on the statistics of other modes. Such interactions are not predicted by the equilibrium statistical theory, since in statistical predictions in Eqs. (10) different modes appear to be completely uncoupled. On the other hand, the overall trend of these interactions is to improve mixing and reduce the non-Gaussian effects of the topography.

IV. STATISTICAL BEHAVIOR FOR $\beta \neq 0$, $U \neq 0$

In this section, we consider the full quasigeostrophic model with variations of the Coriolis parameter, i.e., $\beta \neq 0$ and mean flow $U \neq 0$. To demonstrate the robustness of the non-Gaussian behavior and the influence of geophysical effects, we consider both the small-size truncation T_6 and larger truncation sizes T_{15} and T_{20} .

A. Smaller truncation size T_6

To analyze the Gaussian behavior of the truncated system in the presence of the mean flow, U , and Coriolis force, β , we consider the same multimode topography (22) as in Sec. III C with

$$H_0 = 0.67, \quad M_0 = 0, 1, 2, 3.$$

The values of the other parameters are chosen to be

$$\alpha = 1, \quad \mu = 2, \quad \beta = 0.5. \quad (23)$$

The values of α and μ are identical to the values of these parameters [cf. with Eq. (17)] in the simulations in the preceding sections with $\beta=U=0$. A typical energy spectrum is presented in Fig. 6. Recall that truncated barotropic quasi-geostrophic equations can be rewritten through the Fourier coefficients of the stream function as in Eq. (2). The equations in (2) are considered on the truncation T_Λ with $\Lambda=6$. Numerical simulations are initialized on the energy-entropy level consistent with constraints in Eqs. (12) and (13), which yields the equilibrium statistical predictions in Eqs. (9) and (10). Similar to other sections, all statistics are computed as time averages from a single microcanonical realization with $T=495000$.

Comparison of the statistical behavior of the Fourier components $\psi_{1,0}$ and $\psi_{1,1}$ with and without U and β is presented in Table III and Fig. 7. Similar to other cases, means and variances are sufficiently close to the predictions of the

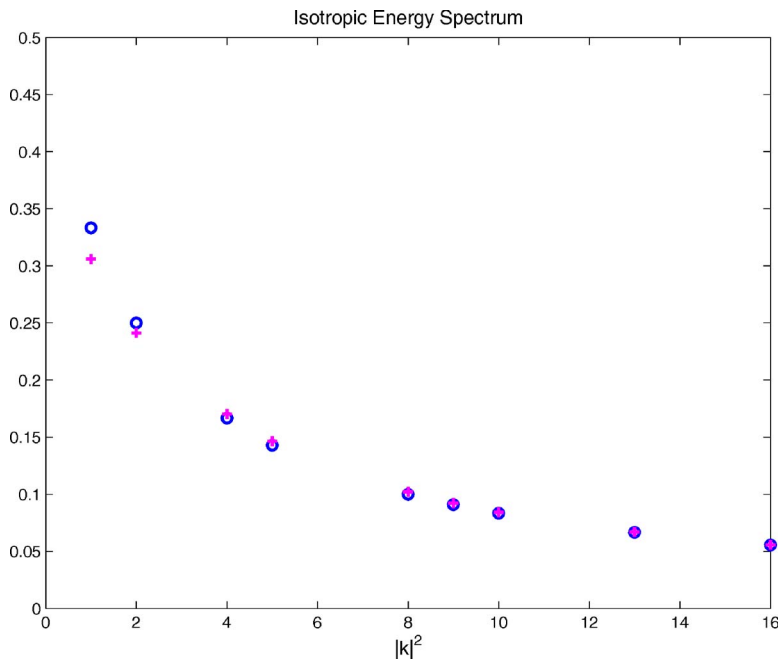


FIG. 6. (Color online) Isotropic energy spectrum ($|k|^2 \langle |\psi_k|^2 \rangle$) in simulations of the truncated system in (2) ($U, \beta \neq 0$) with parameters in (23) and multimode topography in (22) with $M_0=1$. Circles, predictions of the equilibrium statistical mechanics; crosses, numerical simulations.

equilibrium statistical theory. This is illustrated by the behavior of the mean of the mode $\psi_{1,1}$ (bottom left part of Fig. 7), which is unaffected by the presence of geophysical effects and exhibits a linear growth proportional to the magnitude of the topographic mode $h_{1,1}$. Moreover, interactions of frequencies (1,0) and (1,1) reduce the mean of the Fourier mode $\psi_{1,0}$ by approximately 1% or 2%. On the other hand, the

presence of the Coriolis parameter and the mean flow reduces the non-Gaussianity of $\psi_{1,0}$ and $\psi_{1,1}$ by approximately 15% and 10%, respectively. This demonstrates that interactions with additional degrees of freedom in the equations reduce the topographic non-Gaussian statistical effects, but the statistical behavior of means and variances of ψ_k remains nearly unaffected by U and β .

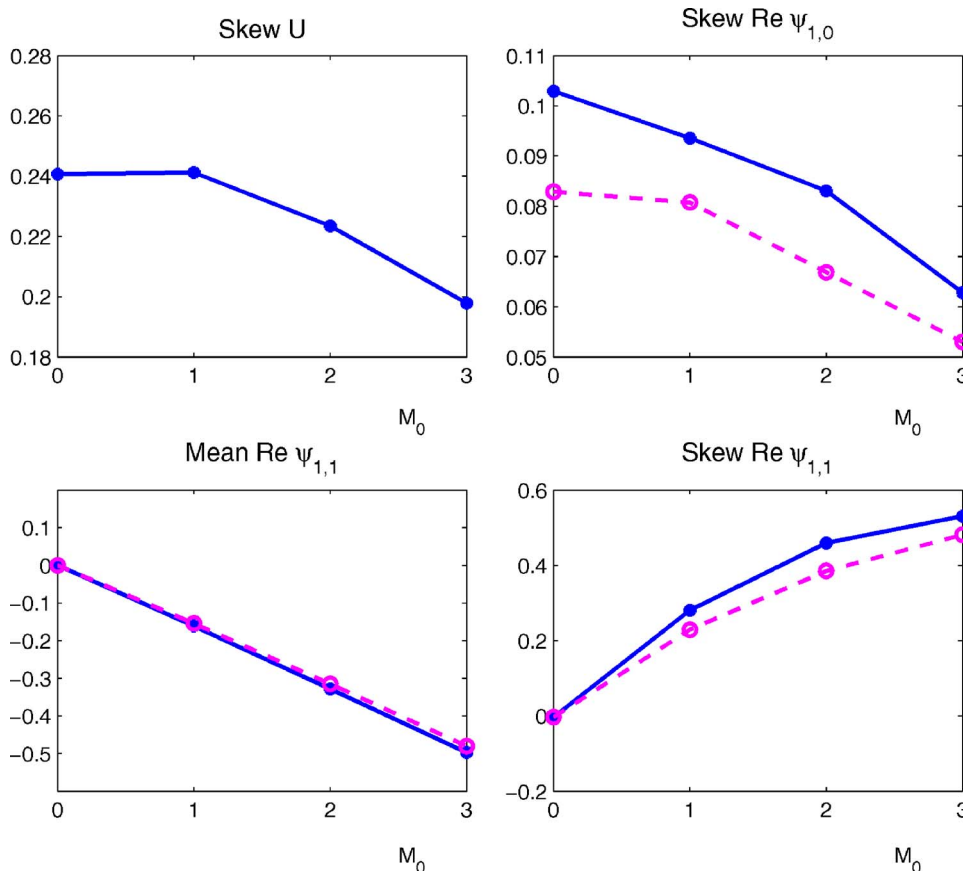


FIG. 7. (Color online) Comparison of simulations with the multimode topography in (22) with and without U, β . Top left: Skewness of U vs the magnitude of the topographic (1,1), M_0 . Top right: Skewness of $\text{Re } \psi_{1,0}$; solid line, simulations with the mean flow, U and β ; dashed line, comparison with simulations with $U=\beta=0$. Bottom left and right: Mean and skewness of $\text{Re } \psi_{1,1}$, respectively. Solid line, simulations with $U, \beta \neq 0$; dashed line, comparison with simulations with $U=\beta=0$.

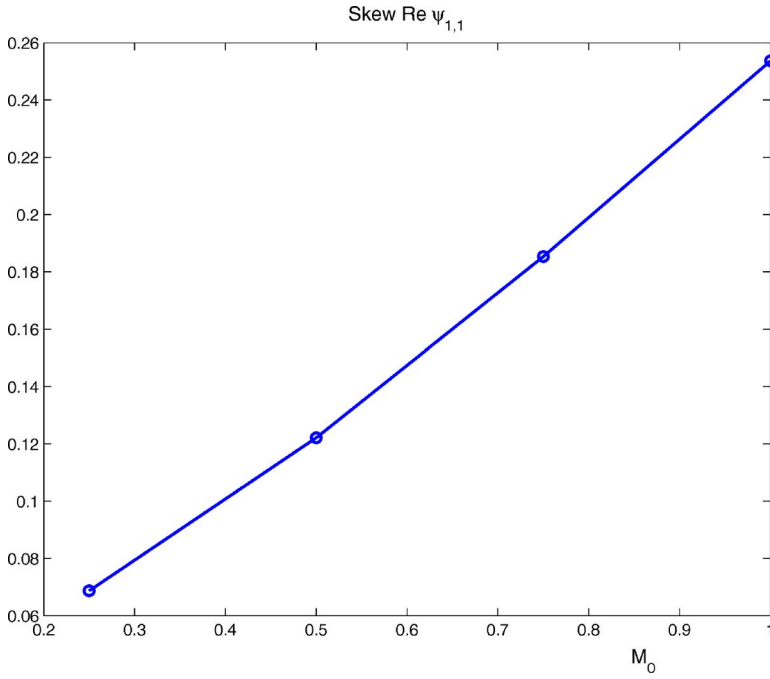


FIG. 8. (Color online) Skewness of the Fourier component $\text{Re } \psi_{1,1}$ vs the magnitude of the topographic mode (1,1), M_0 , in simulations with the truncation size T_{15} and multimode topography in (24).

The equilibrium statistical predictions for the mean flow in Eq. (9) with parameters in Eq. (23) are

$$\text{StatMech Mean } U = -0.25, \quad \text{StatMech Var} U = 0.5.$$

All statistics of the mean flow are affected considerably by the growth of the topographic mode $h_{1,1}$. Fluctuations of the mean and variance of U are approximately 15% for the four simulations with different values of M_0 . Moreover, since the mean flow is driven linearly by the small-scale flow, the non-Gaussian effects “propagate” into the statistical behavior of U as well. Nevertheless, the non-Gaussian behavior of U does not seem to be “additive.” Both third moments of $\text{Re } \psi_{1,0}$ and $\text{Re } \psi_{1,1}$ are positive, but the skewness of U decreases for sufficiently large values of M_0 .

B. Simulations with larger truncation sizes T_{15} and T_{20}

In this section, we verify our findings for truncated systems of larger sizes. In particular, we consider the spectral truncation of the equation in (14) with truncation sizes

$$\Lambda = 15, 20.$$

We would like to emphasize that the corresponding number of real degrees of freedom in these systems is 481 and 841 for $\Lambda=15$ and 20, respectively. We utilize the following multimode topography in the simulations:

$$\begin{aligned} h(x,y) = & 0.5[\cos(x+2.31) + \sin(x+0.11)] + 0.5[\sin(2x \\ & + 0.3) - \cos(2x-1.7)] + M_0[\cos(x+y+2.8) \\ & - \sin(x+y+1.55)] + 0.075[\cos(3x+y-3.1) \\ & + \sin(3x+2y+2.1)] + 0.041[\cos(5x+2y+7.3) \\ & - \sin(4x-2y-0.75)]. \end{aligned} \quad (24)$$

The large-scale modes of this topography are similar to the multimode topography considered in Eq. (22). In addition,

higher topographic wavenumbers (3,1), (3,2), (5,2), and (4, -2) are also added to ensure larger numbers of interactions between the mean flow, U , and the stream function, ψ_Λ . Similar to other sections, we consider the energy-ensrophy level given by

$$\alpha = 1, \quad \mu = 2, \quad \beta = 0.5. \quad (25)$$

To demonstrate the robustness of the phenomena described in the previous sections, we consider topographies in Eq. (24) with increasing magnitude for the mode $h_{1,1}$ for $\Lambda=15$, but due to the increasing computational complexity of the problem, we performed only one simulation with the truncation size $\Lambda=20$. To summarize, we investigated the behavior of the system for

$$\Lambda = 15, \quad M_0 = 0.25, 0.5, 0.75, 1;$$

$$\Lambda = 20, \quad M_0 = 0.5.$$

The behavior of the skewness for the coefficients $\psi_{1,1}$ and the mean flow, U , are depicted in Figs. 8 and 9, respectively. Similar to results described earlier, the third moment of the stream-function coefficient $\psi_{1,1}$ grows linearly with M_0 . Due to the relatively small magnitude of this topographic mode, we do not observe the saturation of the third moment with M_0 (cf. with the bottom right part of the Fig. 7, for example). This is consistent with the results for the single-mode topography described in Sec. III A. The skewness of the mean flow, U , exhibits a nonuniform behavior, where the fast initial growth changes into a slower decay for larger values of M_0 . This is consistent with the statistical behavior of the mean flow for smaller truncation size described in Sec. IV A. In particular, we would like to emphasize that the absolute values of the skewness are approximately comparable for the T_6 (Sec. IV A) and T_{15} truncation sizes.

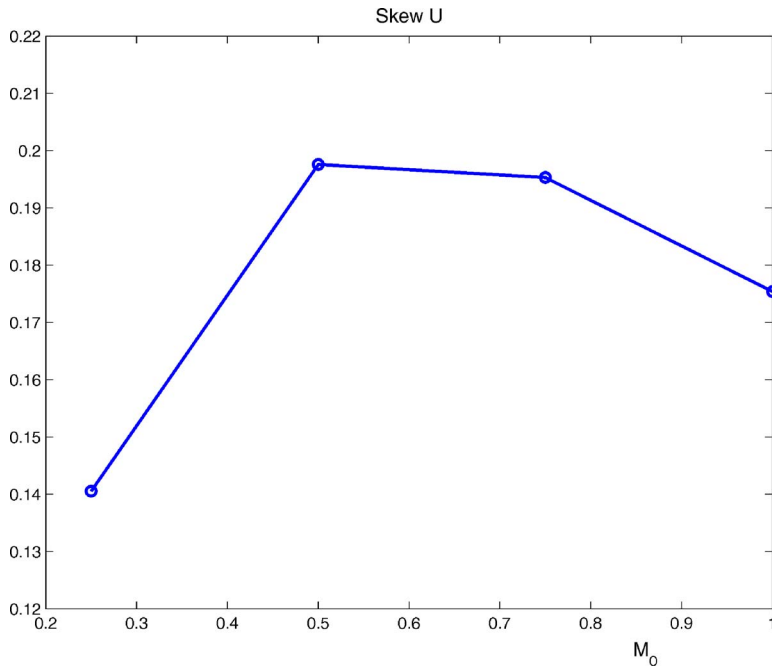


FIG. 9. (Color online) Skewness of the mean flow U vs the magnitude of the topographic mode (1,1), M_0 , in simulations with the truncation size T_{15} and multimode topography (24).

The statistical properties of the mean flow, U , and the first few coefficients of the stream function for the truncation size T_{20} are presented in Table IV. The statistical properties of the mode $\text{Re } \psi_{1,1}$ and the mean flow U are comparable for truncation sizes $\Lambda=15$ and 20. This happens, probably, due to the particular $|k|^{-2}$ shape [see Eq. (12)] of the energy spectrum in the problem. In particular, for the parameter values

$$\alpha = 1, \quad \mu = 2, \quad \beta = 0.5,$$

the total energy given by Eq. (12) is

$$E_{\Lambda=15} \approx 6.74, \quad E_{\Lambda=20} \approx 7.61.$$

Therefore, although the difference in the total number of degrees of freedom between truncation sizes $\Lambda=15$ and 20 is considerable, changes in the total energy are much smaller percentagewise. Thus, numerical simulations with larger truncation sizes suggest that higher wavenumbers have a rather limited affect on the statistical properties of large-scale structures. In addition, we would like to comment that the robustness of the results reported here was verified against simulations with smaller time step and longer integration times.

TABLE IV. Statistics of the Fourier components $\psi_{1,0}$, $\psi_{1,1}$, and the mean flow U in simulations with the truncation size T_{20} and topography (24) with $M_0=0.5$.

	Mean	Variance	Skewness
Re $\psi_{1,0}$	-0.0448	0.1511	0.0335
Re $\psi_{0,1}$	-0.0058	0.1537	0.0070
Re $\psi_{1,1}$	-0.1166	0.0591	0.1314
Re $\psi_{1,-1}$	-0.0019	0.0602	0.0082
U	-0.2326	0.4004	0.2059

C. Simulations with truncation size T_{15} on higher energy-entropy levels

To investigate the generality of the results presented in the previous sections, we also performed simulations with higher energy and entropy levels. In particular, we investigate the behavior of the systems in Eq. (14) with the truncation size T_{15} , multimode topography in Eq. (24), and parameters

$$\alpha = 1, 0.75, 0.5, 0.25, \tag{26}$$

$$M_0 = 0.5, \quad \mu = 2, \quad \beta = 0.5,$$

and

$$M_0 = 0.5, 1, 1.5, 2, 2.5, \tag{27}$$

$$\alpha = 0.5, \quad \mu = 2, \quad \beta = 0.5.$$

From Eqs. (9) and (10), the variance of the mean flow, U , and the Fourier coefficients of the stream function are proportional to α^{-1} . Therefore, smaller values of α correspond to higher energy-entropy levels and larger variance of ψ_k and U . Corresponding fluctuating energy-entropy levels in Eqs. (12) and (13) are

$$E_{\alpha=1, 0.75, 0.5, 0.25} = 6.67, 8.9, 13.35, 26.77,$$

$$\mathcal{E}_{\alpha=1, 0.75, 0.5, 0.25} = 226.89, 302.52, 453.79, 907.58.$$

For a fixed topography, the skewness of the coefficient $\psi_{1,1}$ decays for higher energy-entropy levels (smaller values of the parameter α). This behavior is depicted in Fig. 10. The statistical behavior of the mean flow, U , follows a similar trend. On the other hand, on a fixed energy-entropy level (α , μ , and β are fixed), the non-Gaussian behavior of the stream function seems to be strongly affected by the magnitude of the corresponding topographic mode even for higher

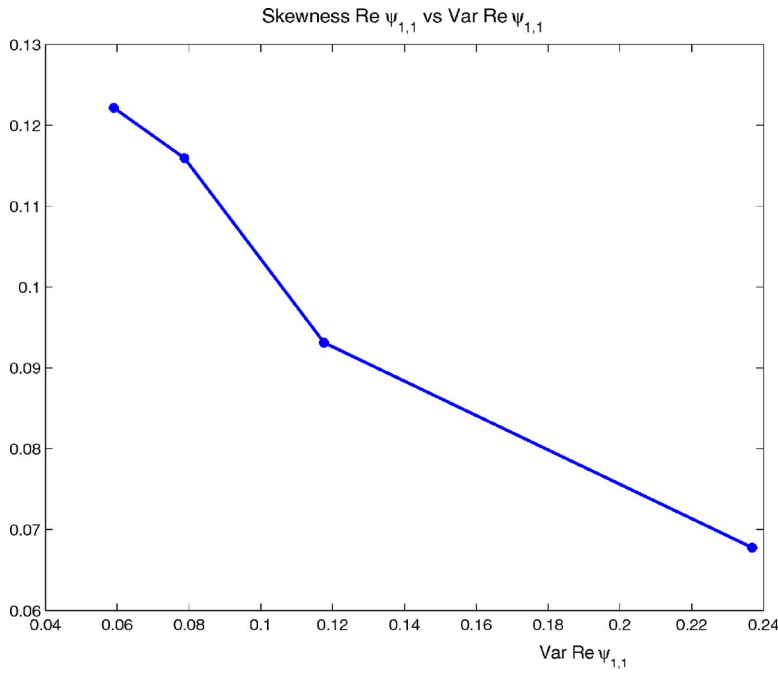


FIG. 10. (Color online) Skewness of $\text{Re } \psi_{1,1}$ vs the variance of $\text{Re } \psi_{1,1}$ in simulations with the truncation size T_{15} and multimode topography (24) with $M_0=0.5$ on energy-entropy levels determined by Eqs. (12) and (13) with $\alpha=1, 75, 0.5, 0.25$.

energy levels. In particular, the linear dependence of the skewness of $\text{Re } \psi_{1,1}$ on the magnitude of the corresponding topographic mode is depicted in Fig. 11. Therefore, on the one hand, larger fluctuations decrease the non-Gaussian affect of topographic modes, but, on the other hand, in systems with larger energy-entropy levels, it is possible to select a topography with a large enough magnitude that will have a significant influence on the non-Gaussian behavior of the stream function. We would like to comment that the statistical behavior of the mean flow, U , is affected much weaker by $h_{1,1}$ on a higher energy-entropy level ($\alpha=0.5$) than on the lower one ($\alpha=1$). In particular, in simulations with parameters in Eq. (27), the skewness of the mean flow is nearly

constant. Therefore, we expect that the statistical behavior of the mean flow, U , will be nearly Gaussian on higher energy-entropy levels regardless of the magnitude of the topography.

V. CONCLUSIONS

The role of the underlying bottom topography is systematically studied for several low-dimensional conservative truncations of the barotropic quasigeostrophic model in a doubly periodic geometry. It is demonstrated that in the absence of the topography, the statistical behavior of the Fourier coefficients is Gaussian and predictions of the equilib-

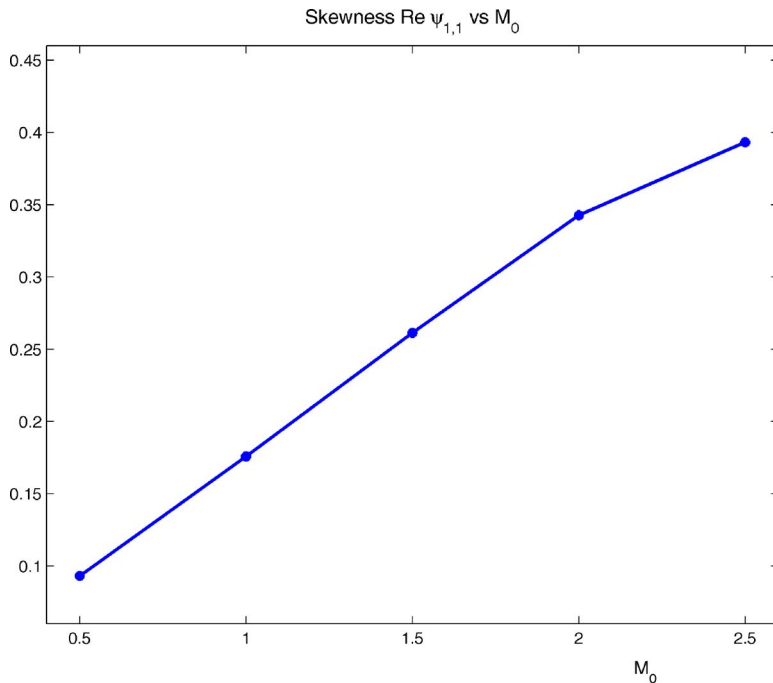


FIG. 11. (Color online) Skewness of $\text{Re } \psi_{1,1}$ vs the magnitude of $\text{Re } h_{1,1}$, M_0 , in simulations with the truncation size T_{15} and multimode topographies (24) with $M_0=0.5, 1, 1.5, 2, 2.5$ on the energy-entropy level determined by Eqs. (12) and (13) with $\alpha=0.5$.

rium statistical theory with two conserved quantities (energy and enstrophy) are in very good agreement with microcanonical simulations.

When topographic frequencies are present in the system, they induce a significant departure from Gaussianity in corresponding Fourier modes of the stream function. The non-Gaussian effect is manifested most strongly for the third moments of the distribution. The non-Gaussian response is linear for small magnitudes of the topography, but saturates for larger topographies. Additionally, non-Gaussian features also become less pronounced as the size of the truncation increases while the topographic magnitude is kept constant. Therefore, for fixed topographies we can expect a near-Gaussian behavior in systems of larger sizes.

Examples presented in Sec. III C demonstrate a non-trivial interaction mechanism between multiple topographic modes. While the equilibrium statistical predictions for a particular stream function coefficient (e.g., $\psi_{1,0}$) are unaffected by the presence of other topographic frequencies, microcanonical simulations with multimode topographies demonstrate that additional topographic frequencies reduce the overall non-Gaussian effect. Furthermore, this observation is also supported by simulations with the mean flow, U , in Sec. IV. The skewness of both Fourier modes, $\psi_{1,0}$ and $\psi_{1,1}$, is significantly smaller in simulations when U and β are present. This indicates that interactions with additional degrees of freedom improve the mixing properties of the model and reduce the non-Gaussian effects of the topography.

Statistical behavior of the mean flow, U , is also affected strongly by the presence of multiple topographic modes. Both the mean and the variance of U exhibit significant fluctuations in simulations with the multimode topography with varying magnitude of $h_{1,1}$. The non-Gaussian behavior of the stream function “propagates” into the mean flow and $U(t)$ exhibits significant departures from Gaussianity even for small topographies (e.g., compare skewness of $\psi_{1,0}$ and U in simulations with the multimode topography in (22) with $M_0=0$).

Simulations with larger truncation sizes $\Lambda=15$ and $\Lambda=20$ confirm the strong influence of topographic interactions on the statistical properties of large-scale structures in systems with $O(500)$ degrees of freedom. Although for a fixed topography the non-Gaussian effects decrease for larger fluctuating energy-enstrophy levels, it is possible to select for each energy-enstrophy level a topography of a larger magnitude that will result in a distinct non-Gaussian behavior of the stream function. Therefore, the non-Gaussian behavior seems to be generic for systems with relatively large (compared to the energy-enstrophy level) topographies. In addition, these simulations also indicate that increasing truncation sizes have a very weak affect on the non-Gaussian statistical behavior of the low Fourier components of the stream function and the mean flow, U .

In addition, the robustness of the results reported here was also verified for several different values of energy-enstrophy parameters and magnitudes of the Coriolis forcing. In particular, non-Gaussian features of the statistical behavior of the stream function and the mean flow were verified for $\mu, \alpha=1, 0.5$ and for the negative temperature regime

(without the mean flow) $\mu, \alpha=-0.5, 1$. Although the moments’ magnitudes depend strongly on the particular energy-enstrophy level, overall statistical trends reported in this paper were confirmed in all simulations with different values of parameters μ , α , and β .

Examples in this paper demonstrate significant departures from Gaussian predictions in spectral truncations of the barotropic quasigeostrophic model of moderate sizes. The non-Gaussian behavior is induced by the topographic frequencies and does not interact with the variations of the Coriolis parameter, β . On the other hand, interactions between the topography and the stream function in simulations with multiple topographic frequencies lead to a complex behavior and, overall, reduction of non-Gaussian features of the stream function. It is possible for non-Gaussian topographic effects to play a significant role in the forced/dissipative barotropic quasigeostrophic model, especially with small forcing and strong dissipation, where only a small subset of stream function coefficients is significant. This issue will be analyzed separately in a subsequent paper.

ACKNOWLEDGMENTS

The author would like to thank J. Frederiksen (CSIRO) and A. Majda (NYU) for valuable comments and suggestions. This research is partially supported by NSF Grant Nos. ATM-0417867 and DMS-0405944 and by DOE Grant No. DE-FG02-04ER25645.

- ¹R. Salmon, G. Holloway, and M. C. Hendershott, “The equilibrium statistical mechanics of simple quasi-geostrophic models,” *J. Fluid Mech.* **75**, 691 (1976).
- ²G. Carnevale and J. S. Frederiksen, “Nonlinear stability and statistical mechanics for flow over topography,” *J. Fluid Mech.* **175**, 157 (1987).
- ³J. S. Frederiksen and B. L. Sawford, “Statistical dynamics of two-dimensional inviscid flow on a sphere,” *J. Atmos. Sci.* **37**, 717 (1980).
- ⁴B. L. Sawford and J. S. Frederiksen, “Mountain torque and angular momentum in barotropic planetary flows: Equilibrium solutions,” *Q. J. R. Meteorol. Soc.* **109**, 309 (1983).
- ⁵A. Majda and X. Wang, *Nonlinear Dynamics and Statistical Theories for Basic Geophysical Flows* (Cambridge University Press, Cambridge, 2006).
- ⁶M. DiBattista and A. J. Majda, “An equilibrium statistical theory for large-scale features of open-ocean convection,” *J. Phys. Oceanogr.* **30**, 1325 (2000).
- ⁷J. Miller, P. B. Weichman, and M. C. Cross, “Statistical mechanics, Euler’s equation, and Jupiter’s red spot,” *Phys. Rev. A* **45**, 2328 (1992).
- ⁸M. DiBattista, K. Haven, A. J. Majda, and B. Turkington, “Statistical equilibrium predictions of jets and spots on Jupiter,” *Proc. Natl. Acad. Sci. U.S.A.* **98**, 12346 (2001).
- ⁹E. Kazantsev, J. Sommeria, and J. Verron, “Subgrid-scale eddy parameterization by statistical mechanics in a barotropic ocean model,” *J. Phys. Oceanogr.* **28**, 1017 (1999).
- ¹⁰J. Zou and G. Holloway, “Entropy maximization tendency in topographic turbulence,” *J. Fluid Mech.* **263**, 361 (1994).
- ¹¹W. J. Merryfield and G. Holloway, “Topographic stress parameterization in a quasi-geostrophic barotropic model,” *J. Fluid Mech.* **341**, 1 (1997).
- ¹²J. S. Frederiksen, M. R. Dix, and S. M. Kepert, “Systematic energy errors and the tendency toward canonical equilibrium in atmospheric circulation models,” *J. Atmos. Sci.* **53**, 887 (1996).
- ¹³M. T. DiBattista, A. J. Majda, and J. Marshall, “A statistical theory for the ‘patchiness’ of open-ocean deep convection: The effect of preconditioning,” *J. Phys. Oceanogr.* **32**, 599 (2002).
- ¹⁴L. C. Kells and S. A. Orszag, “Randomness of low-order models of two-dimensional inviscid dynamics,” *Phys. Fluids* **21**, 162 (1978).
- ¹⁵O. H. Hald, “Constants of motion in models of two-dimensional turbulence,” *Phys. Fluids* **19**, 914 (1976).

- ¹⁶R. Abramov and A. J. Majda, "Statistically relevant conserved quantities for truncated quasi-geostrophic flow," Proc. Natl. Acad. Sci. U.S.A. **100**, 3841 (2003).
- ¹⁷R. Abramov and A. J. Majda, "Discrete approximations with additional

- conserved quantities: Deterministic and statistical behavior," Methods Appl. Anal. **10**, 151 (2003).
- ¹⁸G. Holloway, "Eddies, waves, circulation, and mixing: Statistical geofluid mechanics," Annu. Rev. Fluid Mech. **18**, 91 (1986).